

# Steady state anisotropy two-photon microscopy resolves multiple, spectrally similar fluorophores, enabling *in vivo* multilabel imaging

J. Matthew Dubach,<sup>†</sup> Claudio Vinegoni,<sup>†,\*</sup> and Ralph Weissleder

Center for System Biology, Massachusetts General Hospital and Harvard Medical School,  
Richard B. Simches Research Center, 185 Cambridge Street, Boston 02114, USA

\*Corresponding author: [cvinegoni@mgh.harvard.edu](mailto:cvinegoni@mgh.harvard.edu)

Received May 5, 2014; revised June 17, 2014; accepted June 18, 2014;  
posted June 24, 2014 (Doc. ID 211546); published July 25, 2014

The use of spectrally distinguishable fluorescent dyes enables imaging of multiple targets. However, in two-photon microscopy, the number of fluorescent labels with distinct emission spectra that can be effectively excited and resolved is constrained by the confined tuning range of the excitation laser and the broad and overlapping nature of fluorophore two-photon absorption spectra. This limitation effectively reduces the number of available imaging channels. Here, we demonstrate that two-photon steady state anisotropy imaging (2PSSA) offers the capability to resolve otherwise unresolvable fluorescent tracers both in live cells and in mouse tumor models. This approach expands the number of biological targets that can be imaged simultaneously, increasing the total amount of information that can be obtained through imaging. © 2014 Optical Society of America

OCIS codes: (170.0170) Medical optics and biotechnology; (180.4315) Nonlinear microscopy; (110.0180) Microscopy; (170.3880) Medical and biological imaging; (170.0110) Imaging systems; (170.2520) Fluorescence microscopy.  
<http://dx.doi.org/10.1364/OL.39.004482>

Multichannel imaging, which is at the core of modern fluorescence imaging microscopy, is typically achieved through a mixed combination of multi-wavelength excitation and spectrally filtered emission detection using several photodetectors. Developments in recent years have sparked tremendous growth in the color palette available for both *in vitro* and *in vivo* fluorescent imaging. In particular, advances in fluorescent antibody staining and genetically expressed fluorescent proteins have enhanced technical applications allowing for the investigation of different cell-type tracking and studies of cell–cell interaction, tissue morphology, and cellular activity [1].

Two-photon microscopy is a powerful fluorescence imaging modality based on nonlinear light-matter interaction. Often used for *in vivo* imaging, fluorescent excitation lies in the near-infrared region of the spectrum, making this approach less susceptible to scattering and therefore offering deeper tissue penetration. Moreover, the high spatial and temporal resolution and low phototoxicity associated with two-photon microscopy make it ideally suited for subcellular 3D intravital microscopy imaging applications in xenograft tumors, genetically encoded tissue, or injected fluorophores [2]. However, a major limitation, in comparison to traditional single photon imaging, lies in the limited number of fluorophores that can be efficiently excited and resolved without ambiguity, either concurrently or individually. This shortcoming is because of the limited tuning range (690–1040 nm) of commercial infrared high-intensity pulsed lasers, the inability to operate in a multiline operation mode, the temporal cost of tuning the laser wavelength between acquisitions, and the prohibitive cost and complexity of combining multiple pulsed laser lines into a common excitation path [3]. Furthermore, because the most commonly employed fluorophores have broad overlapping two-photon absorption spectra, they cannot be easily separated by excitation wavelength alone.

Subsequently, the number of labels that can be imaged simultaneously based on their spectral properties is often limited to two or three at the most.

So far, several strategies have been investigated to expand the number of fluorescent labels for *in vivo* imaging, but they all suffer from different drawbacks. Excitation and emission spectral-unmixing [4,5], is highly time-consuming and therefore mostly used for fixed tissue imaging. Two-photon wavelength mixing [6] requires a relatively complex optical setup. Fluorescence lifetime imaging microscopy (FLIM) [7–9] often requires longer acquisition times and dedicated acquisition cards.

Steady state anisotropy, or time averaged anisotropy, presents another potential approach to distinguish among multiple fluorophores that are spectrally similar. Anisotropy occurs because the probability of interaction of a fluorescent molecule with a photon is proportional to the square of the scalar product of the molecule's absorption transition dipole moment and the photon's electric field. When polarized light is incident on an ensemble of randomly oriented fluorescent molecules, a photoselection process is introduced with emission preferentially occurring along the emission transition dipole moment. The angular relation between absorption and emission determines the degree of anisotropy ( $r$ ), which is calculated by measuring the fluorescence emission in the planes parallel and perpendicular to excitation polarization. However, molecular rotation during the fluorophore excitation lifetime contributes to emission depolarization in accordance with Perrin's equation [10]

$$\frac{r_0}{r} = 1 + \frac{\tau_f}{\tau_r},$$

where  $r_0$  is the fundamental anisotropy as measured in the absence of rotational diffusion,  $\tau_f$  is the fluorescence lifetime, and  $\tau_r$  is the molecular rotation time. Environmental factors, in particular pH and temperature, may

alter  $\tau_f$  and  $\tau_r$ , respectively, and should be considered in certain biological environments, such as lysosomes. However, the anisotropy of a fluorescent molecule is largely defined by its intrinsic properties: fundamental anisotropy, size, and fluorescence lifetime. Subsequently, in similar environmental conditions, every fluorophore may have a unique anisotropy. Based on this property, Bigelow *et al.* [11] utilized confocal fluorescence anisotropy microscopy to distinguish between fluorescein in solution and GFP expressed in cells, two molecules with almost identical excitation and emission spectra but different fluorescence lifetimes and molecular weight (i.e., rotational diffusion). Alternatively, two-photon polarization microscopy has been used to measure linear dichroism to determine fluorescent protein orientation in cells [12].

Here, we use two-photon steady state anisotropy microscopy (2PSSA) to resolve multiple, spectrally similar fluorophores characterized by different anisotropies, extending the number of tracers currently available for both *in vitro* and *in vivo* fluorescent imaging.

To implement 2PSSA microscopy we used a modified commercially available two-photon imaging platform (FV1000, Olympus, USA) based on an upright BX61-WI microscope [13] (Fig. 1A). Excitation light from a MaiTai DeepSee Ti:sapphire pulsed laser (Spectra Physics) tuned at 910 nm was used to excite the fluorophores present within the samples. A Glan-Thompson polarizer (Newport, USA) and a half-wave plate (Thorlabs, USA)

polarized the excitation light. A water-immersion objective lens with a high numerical aperture and large working distance focused the excitation beam and collected the fluorescence in a nondescanned mode. Emission was separated in two orthogonal linearly polarized states through the use of a polarizing beam splitter, and finally simultaneously detected by two separate photomultiplier tubes.  $G$ -factor calibration and direct comparison between one-photon and two-photon anisotropy measurements in environments with different viscosity have been performed [13]. Because anisotropy values are dependent on temperature, this was kept constant at 37°C for all experiments with the use of a heating plate, an objective heating collar, and a microscope-adapted environmental imaging chamber.

Regardless of excitation, one-photon and two-photon anisotropy can be defined as:

$$r = \frac{I_{\parallel} - GI_{\perp}}{I_{\parallel} + 2GI_{\perp}},$$

where  $I_{\parallel}$  and  $I_{\perp}$  are the intensities of the fluorescence with polarization components parallel and perpendicular to the excitation polarization, and  $G$  is corrective factor defined as the ratio of detection efficiency for the parallel and perpendicular signal components. For a water-based 10  $\mu\text{M}$  fluorescein (Sigma, ex: 910 nm, em: 515 nm) solution, we obtained an anisotropy value of 0.004 in accordance with previously reported measurements [14]. To illustrate the multilabeling principle, images of 10  $\mu\text{M}$  dye solution of fluorescein and fluorescein isothiocyanate (FITC) conjugated dextran (FITC-dextran, Sigma, 500 kD, ex: 910 nm, em: 515 nm), two dyes with identical absorption and emission spectrum (Fig. 1B), are shown in Fig. 1C. The similar spectral properties renders the two dyes indistinguishable when only fluorescence images are obtained (Fig. 1C, top). However, because FITC-dextran is larger, the rate of rotation is significantly slower compared to fluorescein in solution, producing a higher anisotropy. The two fluorophores are then clearly distinguishable as evident from the corresponding anisotropy images (Fig. 1C, bottom). The fluorescence anisotropy was calculated for each image pixel, with the value representing the weighted average anisotropy of all fluorophores within the corresponding voxel. To visualize the different anisotropy values of each pixel a color lookup table was applied (Fig. 1C), mapping intervals of anisotropy to different colors. All anisotropy images were weighted by the corresponding fluorescence images to account for noise induced variations [13].

To extend this approach to *in vivo* and *in vitro* applications for simultaneous imaging, we considered several fluorophores with similar spectra but distinct anisotropy distributions. To characterize fluorophore anisotropy properties under imaging conditions we first imaged each tracer independently *in vitro* or *in vivo* while working at constant temperature (37°C). All animal experiments were performed in accordance with the Institutional Animal Care and Use Committee at Massachusetts General Hospital under isoflurane anesthesia (2 l/min).

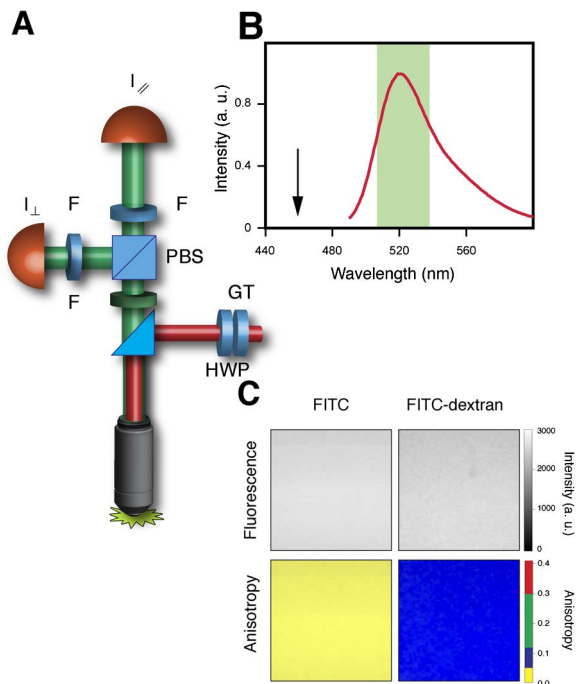


Fig. 1. Two-photon fluorescence anisotropy imaging. A, Schematic illustration of the imaging setup, F:spectral and polarization filters; PBS: polarizing beam splitter; HWP: half wave-plate; GT: Glan-Thompson. B, Emission spectrum for fluorescein and FITC-dextran. Half the wavelength was utilized for two-photon imaging (arrow) and optical emission filter bandwidth (green box). C, Images of fluorescence (top) and anisotropy (bottom) collected in two-photon excitation for a water-based solution of fluorescein and FITC-dextran. Lookup table for color anisotropy assignment is shown on right.

MitoTracker Green (Invitrogen, ex: 910 nm, em: 512 nm) is a fluorophore that preferentially localizes to the mitochondria of live cells. Fluorescence images of HT1080 cells (ATCC), a fibrosarcoma cell line, loaded with MitoTracker Green (1  $\mu$ M for 15 min with 15 min wash) display distinct mitochondria labeling, Fig. 2A, while the corresponding anisotropy image presents an anisotropy distribution between 0.12 and 0.3.

The high molecular weight of FITC-dextran makes it a common vascular dye for microcirculation imaging. Following tail vein injection in a nude mouse (Cox-7, Massachusetts General Hospital), the vasculature was imaged in the ear of the anesthetized animal (Fig. 2B, left). The anisotropy image (Fig. 2B, right) of FITC-dextran in the vascular system presents an anisotropy distribution between 0.05 and 0.12.

Once FITC-dextran leaks out of the vessels, more common in leaky vasculature associated with tumors, it is taken up by phagocytic cells in tumors, predominantly tumor associated macrophages (TAM). To image cellular FITC-dextran we created xenograft tumors in a dorsal skinfold window chamber in nude mice. HT1080 cells were injected subcutaneously and tumors were grown for 1-2 weeks. The cells consisted of a 10:1

mixture of HT1080 cells:HT1080 cells expressing GFP labeled H2B (HT1080 GFP, ex: 910 nm, em: 510 nm) in the nucleus. Tumor bearing mice were intravenously injected with FITC-dextran and imaged 24 h later, allowing FITC-dextran to accumulate in TAMs. In the outer area of the tumor, where only TAMs were present, fluorescence and anisotropy images of FITC-dextran labeled TAMs indicate a distribution of anisotropy between 0.2 and 0.3 (Fig. 2C). The increased anisotropy of FITC-dextran in TAMs over vasculature is likely because of the decreased pH and higher viscosity present in phagocytic vesicles, making FITC-dextran an ideal candidate to separately distinguish the two. Lastly, we imaged HT1080 GFP cells present within the center of the xenograft tumors described above. Anisotropy distribution of GFP (Fig. 2D) was found to be between 0.3 and 0.42.

Although the emission spectrum of all the fluorescent tracers used here (FITC-dextran, GFP, and MitoTracker) overlaps significantly and cannot be resolved by standard fluorescence two-photon imaging (Fig. 2, left column), their anisotropy values in the desired environments are clearly distinguishable (Fig. 2, right column). Therefore, differences in anisotropy of these fluorescent tracers might be used to distinguish them within a single image both *in vitro* and *in vivo*.

To explore the possibility of resolving multiple fluorophores based on their anisotropy values in live cells, we imaged HT1080 GFP cells that were also loaded with MitoTracker Green. Since the two fluorescent tracers overlap spectrally, they cannot be separated from each other in a conventional two-photon fluorescence image (Fig. 3A). However, when the anisotropy values of the image are considered, the MitoTracker Green and GFP can be resolved by assigning a different color to the anisotropy ranges previously determined, providing distinction between nucleus and mitochondria. We then determined if anisotropy imaging could be used to distinguish and resolve multiple spectrally similar tracers *in vivo*. A tail vein injection of FITC-dextran was administered to visualize vasculature within a tumor comprised of HT1080 GFP cells in a mouse dorsal skinfold chamber (see above). The anisotropy values were then used to assign each pixel with fluorescence intensity as corresponding to GFP or FITC-dextran, based on value ranges previously determined for GFP and FITC-dextran (Fig. 2). This approach separates the FITC-dextran labeled vasculature from nuclear GFP present within the tumor cells (Fig. 3B).

We then expanded the number of anisotropy resolvable tracers by imaging tumors 24 h after FITC-dextran injection in order to label the TAMs. Following a second FITC-dextran tail vein injection, to label the vasculature, we imaged the periphery of the tumor, where TAMs accumulate. The emission overlap between the tracers prevents separation of vasculature, tumor cells and macrophages using two-photon fluorescence intensity images (Fig. 3C, left). However, when anisotropy images are taken and anisotropy values are encoded through a lookup table using predetermined value ranges (Fig. 2), vasculature (blue), macrophages (yellow), and GFP labeled cancer cells (red) could be clearly separated, Fig. 3C.

In conclusion, we demonstrate that 2PSSA microscopy can be used to distinguish multiple fluorophores with

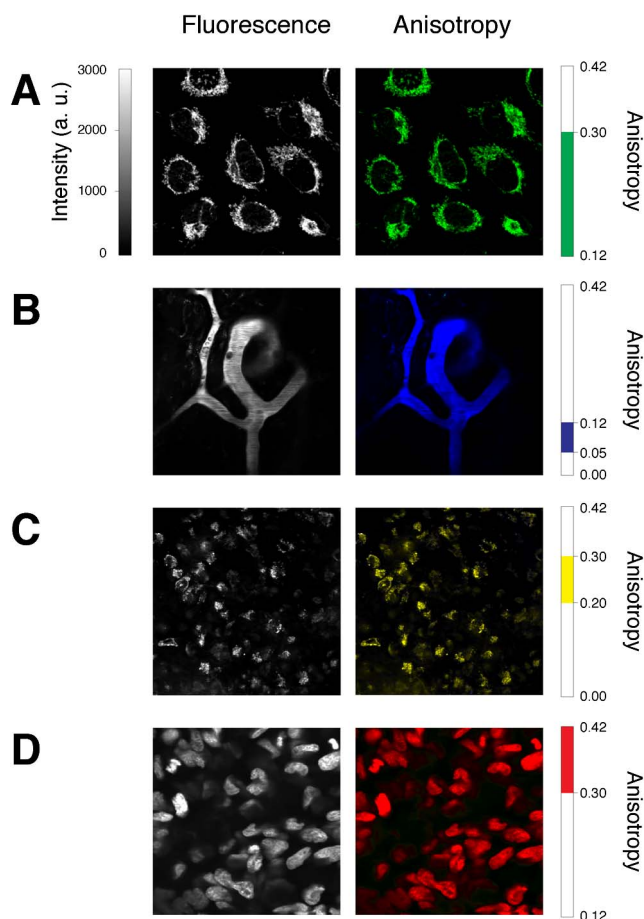


Fig. 2. Two-photon *in vivo* and *in vitro* fluorescence (left) and anisotropy (right) images of A, MitoTracker Green in HT1080 cells; B, FITC-dextran in mouse ear vasculature; C, FITC-dextran in tumor associated macrophages; and D, GFP expressing HT1080 cells in a tumor. Lookup tables for anisotropy color assignments are shown on right.

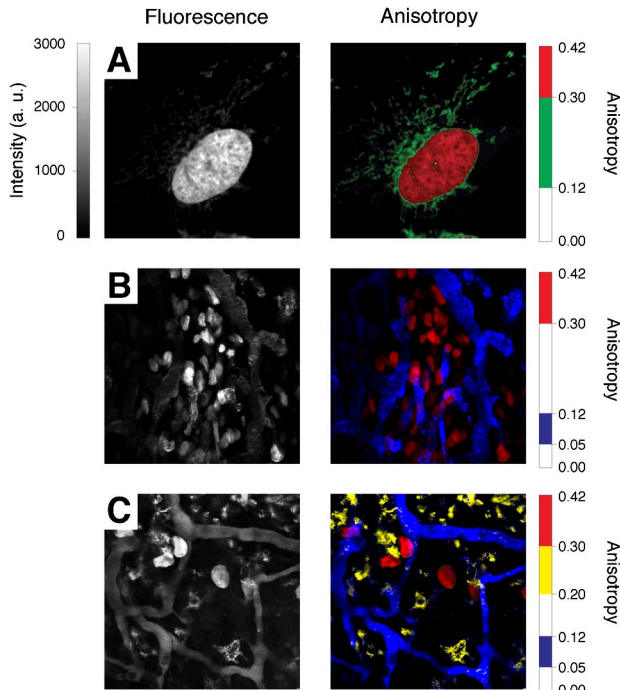


Fig. 3. Simultaneous multilabel imaging by 2PSSA microscopy (left, fluorescence; right, anisotropy). A, *In vitro* imaging of HT1080 GFP cells loaded with MitoTracker Green. B, Maximum intensity projection image stack of an HT1080 GFP tumor implanted in a skinfold dorsal window chamber with FITC-dextran vascular perfusion. Red, GFP; blue, FITC-dextran. C, Maximum intensity projection image stack at the periphery of an HT1080 GFP tumor in a mouse vascularly injected with FITC-dextran 24 h before and during imaging. Red, GFP; blue, vascular FITC-dextran; yellow, tumor associated macrophages FITC-dextran. Lookup tables for anisotropy color assignments are shown on right.

similar emission spectra based on their respective anisotropy values, therefore expanding the number of available reporters that can be used as distinct labeling agents. While we demonstrate simultaneous *in vivo* imaging of three separate channels using tracers in the green emission channel, the approach can be expanded to other fluorophores with any excitation and emission wavelengths. One caveat with the method arises if multiple labels are present within the same voxel. Given the

additive nature of anisotropy, each pixel will represent a concentration weighted average of the present tracers, which may result in an erroneous assignment if multiple fluorophores with different anisotropies exist. The enhanced axial resolution in two-photon microscopy, however, prevents false assignment from being as significant as possible in contrast to confocal or wide-field microscopy.

This project was funded in part by Federal funds from the National Heart, Lung, and Blood Institute, National Institutes of Health, Department of Health and Human Services (under Contract No. HHSN268201000044C), National Cancer Institute (T32CA079443 and P50CA086355), and from the Institute of Biomedical Engineering (under R01EB006432), and in part by 1R01CA164448-01.

†These authors contributed equally to this work.

## References

1. N. C. Shaner, P. A. Steinbach, and R. Y. Tsien, *Nat. Methods* **2**, 905 (2005).
2. M. J. Pittet and R. Weissleder, *Cell* **147**, 983 (2011).
3. D. Entenberg, J. Wyckoff, B. Gligorijevic, E. T. Roussos, V. V. Verkhusha, J. W. Pollard, and J. Condeelis, *Nat. Protoc.* **6**, 1500 (2011).
4. M. H. Brenner, D. Cai, J. A. Swanson, and J. P. Ogilvie, *Opt. Express* **21**, 17256 (2013).
5. A. J. Radosevich, M. B. Bouchard, S. A. Burgess, B. R. Chen, and E. M. Hillman, *Opt. Lett.* **33**, 2164 (2008).
6. P. Mahou, M. Zimmerley, K. Loulier, K. S. Matho, G. Labroille, X. Morin, W. Supatto, J. Livet, D. Debarre, and E. Beaurepaire, *Nat. Methods* **9**, 815 (2012).
7. H. Brismar and B. Ulfhake, *Nat. Biotechnol.* **15**, 373 (1997).
8. K. Carlsson and A. Liljeborg, *J. Microsc.* **191**, 119 (1998).
9. J. D. Driscoll, A. Y. Shih, S. Iyengar, J. J. Field, G. A. White, J. A. Squier, G. Cauwenberghs, and D. Kleinfeld, *J. Neurophysiol.* **105**, 3106 (2011).
10. F. Perrin, *J. Phys. Radium* **7**, 390 (1926).
11. C. E. Bigelow, D. L. Conover, and T. H. Foster, *Opt. Lett.* **28**, 695 (2003).
12. J. Lazar, A. Bonder, S. Timr, and S. J. Firestein, *Nat. Methods* **8**, 684 (2011).
13. J. M. Dubach, C. Vinegoni, R. Mazitschek, P. F. Feruglio, L. Cameron, and R. Weissleder, *Nat. Commun.* **5**, 3946 (2014).
14. J. R. Lakowicz, *Principles of Fluorescence Spectroscopy* (Springer, 2006).